Available online at www.sciencedirect.com

ScienceDirect

MATTER AND RADIATION AT EXTREMES

Matter and Radiation at Extremes 3 (2018) 145−158

www.journals.elsevier.com/matter-and-radiation-at-extremes

Review article

Influence of structural factors on the strength properties of aluminum alloys under shock wave loading

S.V. Razorenov [a,b]

[a] *Institute of Problems of Chemical Physics RAS, Chernogolovka, Russia*
[b] *National Research Tomsk State University, Tomsk, Russia*

Received 22 November 2017; revised 12 February 2018; accepted 19 March 2018
Available online 15 June 2018

Abstract

The results of measurements of the strength characteristics - Hugoniot elastic limit and spall strength of aluminum and aluminum alloys in different structural states under shock wave loading are presented. Single-crystals and polycrystalline technical grade aluminum A1013 and aluminum alloys A2024, AA6063T6, A1421, A7, A7075, A3003, A5083, AA1070 in the initial coarse-grained state and ultrafine-grained or nanocrystalline structural state were investigated. The refinement of the grain structure was carried out by different methods of severe plastic deformation such as Equal Chanel Angular Pressing, Dynamic Channel Angular Pressing, High-Pressure Torsion and Accumulative Roll-Bonding. The strength characteristics of shock-loaded samples in different structural states were obtained from the analysis of the evolution of the free surface velocity histories recorded by means of laser Doppler velocimeter VISAR. The strain rates before spall fracture of the samples were in the range of 10^4-10^5 s^{-1}, the maximum pressure of shock compression did not exceed 7 GPa. The results of these studies clearly demonstrate the influence of structural factors on the resistance to high-rate deformation and dynamic fracture, and it is much less than under the static and quasi-static loading.

PACS codes: 61.82.Bg; 62.50.Ef

Keywords: Aluminum alloys; Shock wave loading; Ultrafine-grained structure; Dynamic strength properties

1. Introduction

The fracture of solids occurs by the nucleation, growth and coalescence of microdefects under the action of tensile stresses. At low rates of fracture, these processes take place near the top of a growing crack or stress concentrators − the potential centers of crack initiation. Under the fast load application, the initiation of fracture is possible simultaneously in a large number of foci and the process acquires the character close to the continual [1]. In this case, the centers of the nucleation of microdefects are the material defects of different structural levels. Relatively large structural defects, such as existing micropores, impurities and grain boundaries, require less stress for their transformation in the centers of fracture than, for example, the accumulation of dislocations or vacancies. As the value of the applied tensile stress gets higher, the smaller (and more numerous) defects become the centers of the nucleation of voids, microcracks and other discontinuities, i.e. with increasing stress, most part of the spectrum of potential sources is involved in the initiation of fracture.

With the growth of the nucleation sites of fracture and their coalescence, the resistance to further fracture decreases. In addition, due to the relaxation of tensile stresses, the growth of relatively small microdefects and the formation of the new ones should be suppressed, and the spectrum of the fracture

E-mail address: razsv@ficp.ac.ru.
Peer review under responsibility of Science and Technology Information Center, China Academy of Engineering Physics.

https://doi.org/10.1016/j.mre.2018.03.004

centers changes in the process of destruction. The growth of microdefects is connected with plastic deformations in their surroundings and, accordingly, should appreciably be controlled by the resistance to plastic deformation.

The study of the processes of high-rate deformation and fracture of metals and alloys allow identifying the spectra of strengthening factors and sources of fracture, thus to obtain the quantitative characteristics of the hierarchy of material structural levels. It is unclear whether there should be a correlation between the spectrum of strengthening factors and foci of fracture, however, for the materials with a distinct hierarchy of structural levels, it is natural to expect that the boundaries of structural levels should correspond to the marked areas in the spectrum of the fracture centers.

The investigations of the mechanical properties of materials under the strain rates $>10^4$ s^{-1} are carried out by the method of shock wave loading of the specimens tested. The technique of shock waves is a powerful tool for studying the material properties at extremely high strain rates with well-controlled loading conditions. The measurement is based on the fact that the wave structure and dynamics of wave interactions are determined, apart from the thermodynamic equations of state of matter, by the processes of elastoplastic deformation and fracture in the material. For the registration of the structure and evolution of intense waves of compression and rarefaction in solids, the methods of continuous recording of the loading history with a high spatial and temporal resolution are developed. Now the methods of analysis of the wave profiles are also well developed and described. With their help, the extensive experimental information about the elastic–plastic and strength properties of technical metals and alloys, geological materials, ceramics, glasses, polymers and elastomers, ductile and brittle single crystals in the microsecond and nanosecond range of durations is obtained. On the base of the experimental data, the phenomenological rheological models of deformation and fracture are developed, which are necessary for calculating the processes of explosion, high-velocity impact, and interaction of powerful pulses of radiation with matter.

Dynamic strength of materials at the fracture in the submicrosecond range of loading durations is investigated by studying the spall phenomena at the reflection of the pulse of one-dimensional shock-wave compression from the free surface of the body [1,2]. The experiments with shock waves are conducted under conditions of uniaxial deformation. The interference of incident and reflected waves leads to the appearance of tensile stresses in the inner sections of the specimen, resulting in a triggered high-rate fracture. Since the critical tensile strength for the ductile metals and alloys is much higher than the yield strength under uniaxial deformation, the fracture occurs at a stress state close to a hydrostatic state. High-rate fracture under the spall is a kinetic process of nucleation, growth and coalescence of numerous microdefects. For this reason, the realized values of tensile stresses defining the material resistance to fracture, as mentioned above, increase with the increasing rate of load application. The value of critical tensile stresses under spall fracture (the spall strength of the material) is determined on the basis of measurements of the free surface velocity as a function of time $u_{fs}(t)$.

The main aspect of the studies of the dynamic material strength is the measurement of dependence of fracture stresses from time or the strain rate, temperature and different material structure. Even most studies of spall fracture are fulfilled for technical metals and alloys, the behavior of high-purity metals and metal single crystals, polymeric materials, ceramics, glasses, high strength single crystals and liquids is also interesting and important. At present time, the information about strength properties of a wide range of technical metals and alloys, metallic single crystals in the microsecond and nanosecond range of exposure durations is obtained. The recent studies focus on the details of the mechanism of the phenomenon and their relationship to material structure in order to find new fields of application of shock waves technology for solving problems of materials science, physics of strength and plasticity. In this short review, by the examples of aluminum and aluminum alloys, the influence of structural factors on resistance to their high-rate deformation and fracture under shock wave loading will be discussed.

2. Experimental methods

For the shock-wave loading of samples, impacts of explosively-launched flyer plates are used, where the source of energy for the initiation of loading pulses is chemical energy high explosives (HE). To simplify the interpretation of the measurement results, a flat stationary shock wave in the samples is generated. The pulses of shock loading with a constant pressure (for some time) behind the shock jump are provided with the plate impact. A sufficiently large transverse size of the impactor and the specimen provides the one-dimensionality of the medium motion during the time interval required for measurements. Under such conditions, the analysis and interpretation of the measurements results are very simple and reliable. To reduce the velocity of a launched plate to less than 1 km/s, the method of the impactor acceleration by the shock wave is used. Such devices are also attractive by the fact that they can be used for accelerating very thin impactors—foils or films, which provides obtaining short (up to nanoseconds) pulses of shock loading [1,2].

To determine the dynamic characteristics of materials tested in this work, a method of continuous measurement of the velocity of matter is used, which allows recording the wave profiles, or in other words, the evolution of the loading pulse during its propagation through the material. The physical basis of the measurement, as mentioned above, is that the wave structure and the dynamics of wave interactions are determined, in addition to the thermodynamic characteristics of the substances or their dynamic compressibility, by the processes of phase and polymorphic transformations of matter in the shock wave and the characteristics of their elastic–plastic deformation and fracture [3,4]. Such measurements have a primary nature, i.e. they are not connected with the construction of the calibration dependence, and therefore have higher accuracy. In experiments discussed in this paper, for the

registration of full wave profiles the symmetric optical laser interferometric velocimeter VISAR (Velocity Interferometric System for Any Reflection) is used, as the most promising tool in relation to high spatial-temporal resolution and accuracy [5]. For this, the measurements take differential characters, which significantly increases the accuracy. The high spatial resolution of the laser methods is ensured by that the probing laser beam is focused on the sample to a spot with a diameter of ~0.1 mm. The minimum registered rise time in front of the shock wave is currently ~1 ns, which is determined by the frequency characteristics of the electronic equipment when fixing the interference fringes by means of electronic photomultipliers.

Practically all the measurement results of the strength characteristics of shock-compressed aluminum alloys presented here are obtained in the experiments on the registration of the full wave profiles, whose schematic is shown in Fig. 1. Thin aluminum impactor with a thickness of 0.2–0.85 mm is accelerated to a velocity of 650 ± 30 m/s by the shock wave generated by the so-called "explosive lens" in a steel attenuator. The evolution (wave profile) of the compressive shock wave in the samples with a thickness of typically 1–3 mm, the analysis of which allows obtaining the desired characteristics of the material, is recorded in the loading process by means of laser velocimeter VISAR. The exact thicknesses of the samples and impactors are specified in the figure captions, where the results of certain experiments are presented. The use of such a loading setup is also connected to the fact that the tested samples after processed by severe plastic deformation generally have small sizes. Accordingly, to maintain one-dimensionality of the process within the required recording time, their thickness is less than 3 mm. The maximum pressure of shock compression in these experiments varies in the range of 5–7 GPa. The rate of deformation of the material before spall fracture of the samples ranges from 5×10^4 to 5×10^5 s^{-1} depending on the sample and impactor thicknesses.

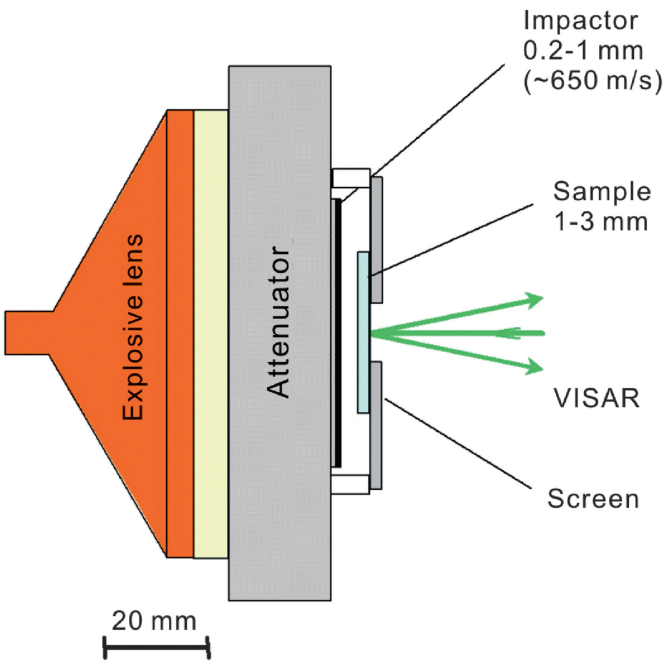

Fig. 1. Schematic of the experiments on the launching of thin aluminum impactors by shock waves generated by explosive devices.

3. Aluminum single crystals

The simplest and clearest examples of the influence of material structure on its strength properties are the measurements of dynamic strength of single crystal metals and their comparison with metals in the polycrystalline state. In Fig. 2, the results of experiments on the measurement of spall strength of the technical aluminum 1013 and of the aluminum single crystal are compared [6]. At the selected ratio of the thickness of the impactor and the sample, the conditions of loading near the free rear surface of the sample correspond to the beginning of shock wave decay under the action of overtaking the rarefaction wave. As a result, the wave profiles obtain the form close to triangular. In Fig. 3, the wave profiles are shown for single-crystal aluminum and commercial aluminum of a purity of 99.9% obtained in the experiments on their loading at the accelerator of light ions "KALIF" by the pulse compression with a duration of about 40 ns [7]. The thickness of the samples in these experiments is 0.43–0.45 mm. The strain rate before the fracture is ~5×10^6 s^{-1}.

The analysis of the experimental wave profiles (Figs. 2 and 3) allows obtaining some important parameters of the loading conditions and strength characteristics of the material resistance to high-rate deformation and fracture. The maximum pressure of shock compression p_{max} is calculated from the maximum of the free surface velocity u_{fsmax} as $p_{max} = \rho_0 u_s u_{fsmax}/2$, where ρ_0 is the initial material density, u_s is the shock wave velocity. To calculate this pressure, shock adiabatics of aluminum is typically used, for example, in the form $u_s = 5.35 + 1.34 u_{fs}/2$ [8].

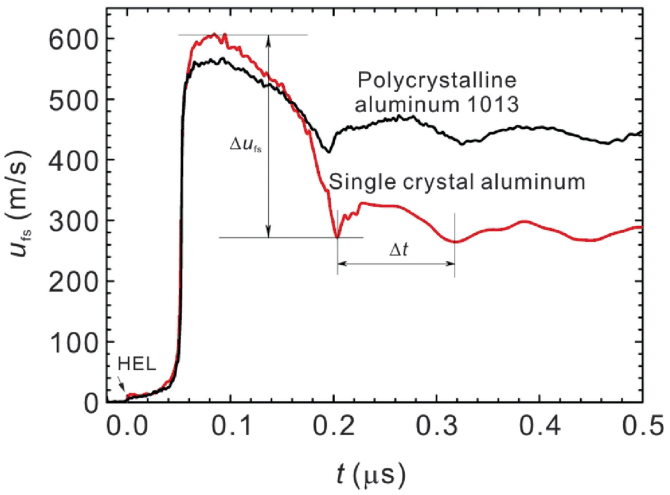

Fig. 2. Profiles of the free surface velocity of samples of technical aluminum 1013 and an aluminum single crystal with a thickness of 2 mm under the impact of an aluminum plate with a thickness of 0.4 mm (~650 m/s) [6].

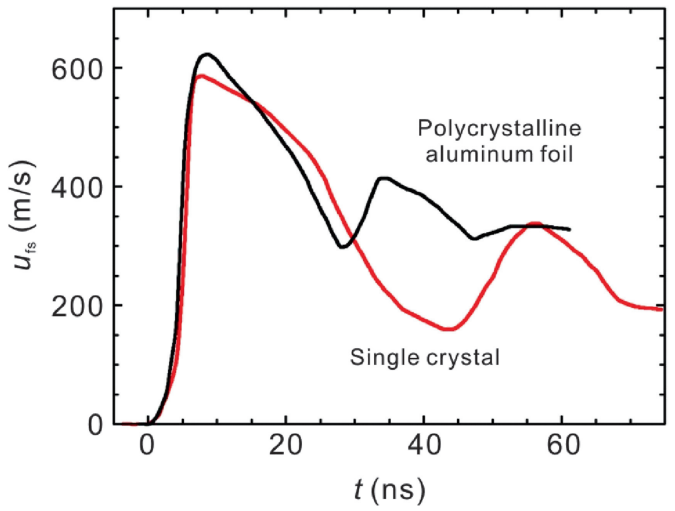

Fig. 3. Results of the registration of the free surface velocity histories of aluminum single crystal and polycrystalline pure aluminum from the experiments with pulse ion beam generator "KALIF" [7]. The direct action of the pulsed ion beam on samples with a thickness of 0.45 mm (single crystal) and 0.43 mm (poly-crystal).

The values of the Hugoniot Elastic Limit (HEL) σ_{HEL} and yield stress Y are calculated according to the amplitude of the elastic precursor front u_{fsHEL} measured from the wave profiles as [1,4]:

$$\sigma_{HEL} = \rho_o c_l u_{fsHEL}/2 \text{ and } Y = \frac{1-2\nu}{1-\nu}\sigma_{HEL} = 2\sigma_{HEL}\left[\frac{c_s^2}{c_l^2}\right] \cong 1.5\sigma_{HEL}\left(1-\frac{c_b^2}{c_l^2}\right),$$

where c_b, c_l, c_s are bulk, longitudinal and shear sound speeds in the material respectively, ν is the Poisson's ratio.

For the calculation of the critical fracture stresses under spall (spall strength) from the experimental profiles of velocity $u_{fs}(t)$, the value of velocity reduction from the maximum to the first minimum at the moment of spall Δu_{fs} was determined. Taking into account the correction for the elastic–plastic behavior of samples of aluminum alloys δ, the value of spall strength σ_{sp} is determined from the relation [1,9]:

$$\sigma_{sp} = 0.5\rho_0 c_b\left(\Delta u_{fs} + \delta\right) \quad \delta = \left(\frac{h_{sp}}{c_b} - \frac{h_{sp}}{c_F}\right)\cdot|\dot{u}_1|c_F = c_b c_l\sqrt{\frac{\dot{\sigma}_{x+} - \dot{\sigma}_{x-}}{\dot{\sigma}_{x+}c_l^2 - \dot{\sigma}_{x-}c_{b-}^2}}$$

where c_F is the speed that corresponds to a distorted velocity profile of the free surface at the moment of spall, $|\dot{u}_1|$ the velocity gradient of the free surface in the unloading section of the incident pulse of compression.

In addition, the wave profiles can be used to obtain data on the thickness of spall plate h_{sp} formed under spall fracture. The thickness is calculated from the ratio $h_{sp} = c_l\Delta t/2$, where Δt is the propagation time of the spall pulse through the spall plate equal to the time of one oscillation of the surface velocity after spalling, which is determined from the wave profiles $u_{fs}(t)$.

The expansion ratio of the substance in the rarefaction wave front before the spall fracture as the strain rate is taken here and defined as [2]:

$$\frac{\dot{V}}{V_0} = -\frac{\dot{u}_{fsr}}{2c_b},$$

where $|\dot{u}_{fsr}|$ is the measured drop rate of the free surface velocity of the sample in the unloading part of the shock compression pulse.

From Fig. 2, it is seen that in the single crystal of aluminum, the implemented fracture stresses under spall, proportional to Δu_{fs}, are more than two times higher than the tensile stresses, leading to the fracture of polycrystalline sample of aluminum 1013. The increase in the strain rate, which is almost two orders of magnitude in experiments on the loading of samples by the pulsed ion beam, results, as expected, in an increase of spall strength of the single crystal and polycrystalline samples (Fig. 3).

The value of fracture stresses under spalling in single crystals is about 3 GPa, whereas in polycrystalline aluminum it does not exceed 2 GPa. The smaller difference in strength is associated with higher strength of high-purity aluminum compared to the technical aluminum 1013. Homogeneous metal single crystals are free from such potential sources of fracture as the grain boundaries, brittle inclusions and micropores, and because of this, it shows a 2–3 times higher spall strength than the same metals in the polycrystalline state. Similar results are obtained for a number of other metals in the single-crystal state [10–15]. But even received for "pure" single crystals, their dynamic strength is sufficiently far from the theoretical strength of these materials, even under ultrashort pulses of compression. At present, in experiments with shock waves, it is possible to measure the level of tensile stresses, comparable with the ultimate or "ideal" strength of condensed matter, determining the upper limit of possible resistance to fracture [16]. As the high-rate spall fracture is a kinetic process of nucleation, the growth and coalesce of numerous microdefects, the realized values of resistance to fracture increase with increasing the rates of load application [1]. So, in the experiments at the loading of the aluminum by laser pulses of femtosecond duration, the spall strength reaches 6 GPa under the strain rate $>10^9$ s^{-1} [17,18]. The maximum possible strength value corresponds to the negative pressure or tensile stress at which the bulk modulus becomes zero. In particular, for aluminum the calculated value of the ideal strength is 11.7 GPa at a temperature of 0 K [19]. From the comparison of these values, it is clear that even at such high rates of fracture, the spall strength reaches values only slightly higher than half of the theoretical strength of aluminum.

4. The influence of mechanical and heat treatment

Another obvious example of the influence of structure is on the strength properties of materials – technological processing of metals such as billets heat treatment (quenching, annealing,

etc.), or preliminary mechanical processing – bulk pressing, extrusion, cutting, rolling and so on [20,21]. Fig. 4 shows the examples of measurements of the free surface velocity profiles of samples of aluminum alloy D16 in the initial (quenched and aged) state (1), in the state after annealing at temperature of 450 °C (2), and in the ultra-fine grained state after multiple overall pressing at the temperature range of 450–200 °C (3) [22]. The hardness of the alloy by Vickers in the initial state is equal to 1100 MPa. The grain size varies from 1 to 20 μm. After annealing, the grain size increases due to the disappearance of the fine fraction with size less than 10 μm, and the hardness of the alloy decreases to 560 MPa. Processing by overall pressing at elevated temperatures leads to the formation of predominantly non-equiaxed grains with a lateral size of 0.2–0.8 μm. The hardness of the alloy decreases due to heating, as a result of the processing by overall pressing increased to 850 MPa. In detail the influence of severe plastic deformation of metals for their resistance to high rate fracture will be discussed below.

At the wave profiles, all the peculiarities of their evolution at the spall fracture of samples are recorded: the exit on the surface of the elastic precursor (HEL), the plastic shock wave and the part of the following rarefaction wave. After reflection of the pulse compression from the free surface, inside the sample the tensile stresses are generated, and as a result, its spall fracture is initiated. This leads to the relaxation of tensile stresses and the compression wave (spall pulse) formation, the output of which on the surface of the sample causes a second rise of its velocity. A weak compression wave before the front of the elastic precursor (marked as AS in Fig. 4) is the result of the action of air shock wave in front of the flying impactor. The rise time of parameters in the plastic shock wave is determined by the material viscosity or relaxation time of the stress.

From the wave profiles shown in Fig. 4, it is clear that the annealed material has the Hugoniot elastic limit (190 ± 20 MPa, $Y = 85 \pm 10$ MPa) more than three times lower than the as-received value (730 MPa, $Y = 310$ MPa). The plastic wave slope, characterizing the rate of compression in the annealed material, is 4–5 times higher than in the as-received state, which indicates a lower viscosity or a smaller relaxation time of deviatoric stress. The annealing leads to a significant drop in spall strength of the material, which is 1.5 ± 0.02 GPa in these conditions for the initial state and 1.2 ± 0.05 GPa after annealing. The refinement of the grain structure as a result of processing of the overall pressing results in an increase in the Hugoniot elastic limit of the annealed material up to 320 ± 20 MPa ($Y = 140$ MPa), but have no significant effect on the value of spall strength (1.35 ± 0.05 GPa). The spall fracture of the alloy in initial state has a delayed character–for a long time after the beginning of the fracture, the spall layer remains connected with the base part of the sample and, consequently, continues to slow down. The deceleration of the spalled plate correlates with the yield strength of the material–for the annealed alloy, the effect is much less. The decrease of grain sizes leads to the accelerated completion of fracture.

The results of the free surface velocity profiles measurements of the samples of 2024 alloy in the direction of rolling and in the transverse direction reveal the influence of technological rolling in this alloy as seen from Fig. 5 [22]. A direct comparison of the wave profiles in Fig. 5 obtained in the loading conditions in the direction of rolling and in the transverse direction shows obviously less resistance to the spall fracture in the latter case. In this respect, the behavior of duralumin 2024 is like the one previously observed for textured steels and alloys [20,23–25]. From the velocity profiles of the free surface presented in Fig. 5, it is clear that the spall fracture of the alloy under the loading in the rolling

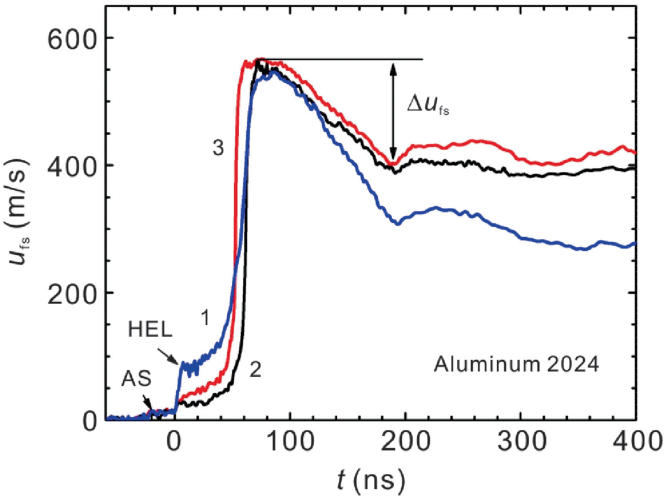

Fig. 4. Free surface velocity histories of samples of aluminum alloy 2024 in the initial (quenched and aged) state (1), the annealed at temperature of 450 °C (2), and with the ultra-fine grained structure after multiple overall pressing at the temperature range of 200–450 °C (3) [22].

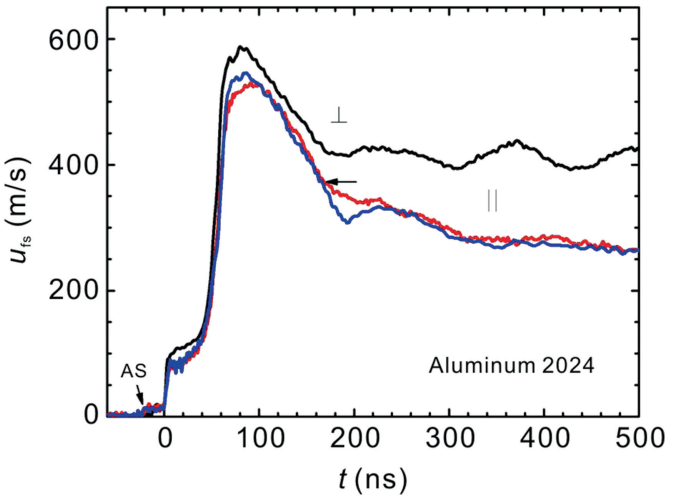

Fig. 5. Profiles of free surface velocity of samples of 2024 alloy with a thickness of 2 mm in as-received state at loading by an impact of aluminum plate with a thickness of 0.4 mm [22]. The signs || and ⊥ mark conditions of loading in the direction of rolling and in the transverse direction, respectively. AS is a result of the impact of air shock wave in front of the plate-impactor. The arrow on the profile without the clear spall pulse marks the expected beginning of fracture.

direction is delayed: for extended periods of time after the beginning of the fracture of a spalling, the surface layer remains connected with the base part of the sample and, consequently, continues to be decelerated. Note that this type of fracture is observed earlier, in particular, in experiments with steel 09G2S [23], loaded, as in our case, in the direction of rolling.

A comparison of the two wave profiles obtained under the same loading conditions (Fig. 5) shows that the found resistance to spall fracture under shock compression in the longitudinal direction varies from one experiment to another. The variations of spall strength values are observed previously [26,27] and are explained by heterogeneity of the material structure. Similar effects can be observed if the spatial resolution of measurements (in this case 0.1 mm) is smaller than the characteristic size of the transverse inhomogeneities of velocities field. Furthermore, the effects of the fracture inhomogenity are smoothed out as the signal propagates from the spall plane to the sample free surface. The thickness of the spalling in these experiments is equal to 0.35 mm. Consequently, one can speak about the typical size of the inhomogenities of the material structure being more or approximately equal to 0.1–0.3 mm. At the same time, the metallographic analysis of the recovered steel samples [23] shows a lack or low degree of coalesce of the formed cracks or pores, at least in the direction perpendicular to the direction of shock loading. Under the transverse impact loading, the fracture is completed faster, while the deceleration of spall plate is practically not observed.

5. Dynamic strength properties of ultrafine-grained aluminum and aluminum alloys

It is known that under conditions of friction, metal processing and other technological processes, the extremely high strain rates up to 10^5 s^{-1} are achieved [28]. Severe plastic deformation under friction leads to the refining of the material grain structure, which in turn causes a change of their mechanical properties. The influence of grain size on the resistance of polycrystalline metals and alloys to the applied loading, such as tension, was observed in the first half of last century and expressed by the well-known dependence of the Hall-Petch [29,30] $\sigma = \sigma_0 + K_1 D^{-1/2}$, where σ_0 and K_1 are the parameters defined for a particular material, and D is its average grain size. E.O. Hall theoretically validated the dependence of the material yield strength from grain size and N.J. Petch confirmed it experimentally on steel samples. Fig. 6 shows the examples of the Hall-Petch dependence for some aluminum alloys in static tests [31].

This effect has led to the fact that in recent decades, new class of materials – the so-called ultrafine-grained (UFG) or submicrocrystalline materials, sometimes called nanocrystalline (NC) with an average grain size of their polycrystalline structure less or much less than one micron, became widespread. Some historical aspects of this field of material science are presented in Ref. [32]. From the 80s of the last century, there began a rapid development of methods and technologies

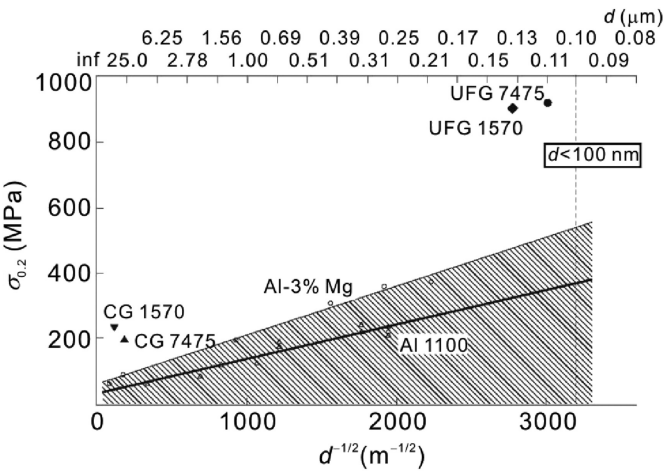

Fig. 6. Hall-Petch dependences for aluminum and aluminum alloys in coarse-grained (CG) and ultrafine-grained (UFG) states [31].

of obtaining such materials, the number of which in different variations and combinations has apparently come to several tens [33]. Each of these methods has its advantages and disadvantages. One of the main problems of these technologies is the problem of manufacturing uniform metal workpieces of materials with ultrafine-grained structure large enough, acceptable for use in various fields of engineering. Of course, the question about their effectiveness – the correspondence of price and quality of the obtained materials arises. Currently, most of the developed methods are still used to obtain small quantities of such materials with the goal of a comprehensive study of their properties. Many studies have shown that the ultrafine-grained materials obtained by severe plastic deformation, with a grain size of one hundred nanometers or even less up to several micrometers possess high strength and other properties attractive for various engineering applications [34–36], which in fact causes a great interest. The same circumstances make relevant the study of the behavior of metallic materials in various states, including ultrafine-grained, at high strain rates under shock wave loading of samples. In this paper, the results of studies of the strength properties under pulse loads of aluminum and aluminum alloys in ultrafine-grained states obtained by different methods of severe plastic deformation are presented.

5.1. Method of equal channel angle pressing

5.1.1. Aluminum alloy AA6063T6

One of the aluminum alloys, which is an object of the study in this work, is thermally hardened aluminum alloy AA6063T6 of system Al-Mg-Si. The alloy contains 98.85% Al, 0.43% Si, 0.52% Mg, 0.16% Fe; its structure and mechanical properties for the initial and ultrafine-grained states at the strain rates up to 10^3 s^{-1} are described in detail in works [37,38]. Ultrafine-grained samples of this alloy were obtained by Equal Channel Angular Pressing (ECAP) after 2 and 8 passes. In the initial state, the average grain size in the alloy was 80–100 μm, while after 2 passes of equal channel angular

pressing, it decreased to 1–1.5 μm, and the increase of the number of passes up to 8 did not lead to further reduction of the grain size, but the disorder of grains increased significantly. The yield strength $\sigma_{0.2}$ of the alloy as a result of intensive plastic deformation was increased by one and a half (from 205 MPa to 305 MPa). In Fig. 7, the results of experiments with dispersion hardened aluminum AA6063T6 in the original heat-treated state and after ECAP (8 passes) are compared.

From the analysis of the wave profiles obtained for the samples of aluminum alloy AA6063T6 of 2 mm thickness in as-received and the UFG states after 2 and 8 ECAP passes, the values of the Hugoniot elastic limit were defined as 180 ± 10 MPa (Y = 82 MPa) for the initial coarse-grained material and 400 ± 20 MPa (Y = 180 MPa) for ultrafine-grained material after severe plastic deformation. The values $\sigma_{0.2}$ evaluated in the approximation of a simple wave were 182 ± 10 MPa and 311 ± 15 MPa, respectively. The data of shock-wave measurements practically coincided with the values of the flow stresses at low strain rates. The value of spall strength increased from 1.28 GPa to 1.48 GPa with decreasing grain size. At the same time, judging by the slope and amplitude of the spall pulse, the fracture rate of the ultrafine-grained material was slightly higher than that of the as-received one.

Figs. 8 and 9 present the summarized results of the decay of elastic precursor depending on the passed distance and the spall strength depending on the strain rate in the rarefaction wave for AA6063T6 aluminum alloy in different structural states together with the results of similar measurements for aluminum and other aluminum alloys. From Fig. 8, it is seen that the studied alloy demonstrates a high HEL, which grows with the grain size decreasing. Its significant increase is observed in the samples after 8 ECAP passes. As for other aluminum alloys, the values of the Hugoniot elastic limit clearly decrease with the passed distance.

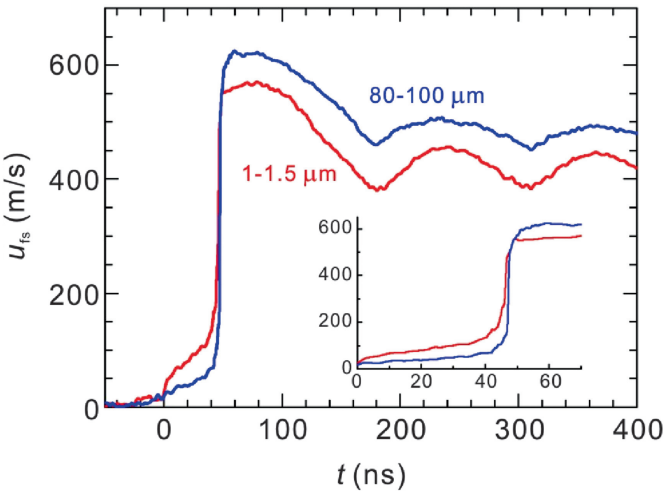

Fig. 7. Wave profiles obtained in experiments with samples of 2 mm in thickness in as-received and ultrafine-grained structural states of aluminum 6063T6 after 8 passes ECAP under loading by the aluminum impactor of 0.4 mm at the velocity of ~660 m/s. The values of the grain sizes in μm are given near the waveforms.

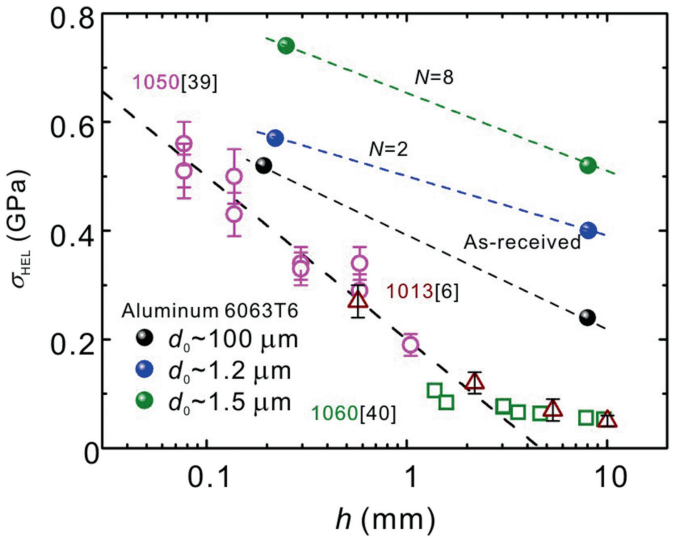

Fig. 8. Decay of the elastic precursor in the samples of aluminum alloy 6063T6 supplemented with the published data [6,39,40].

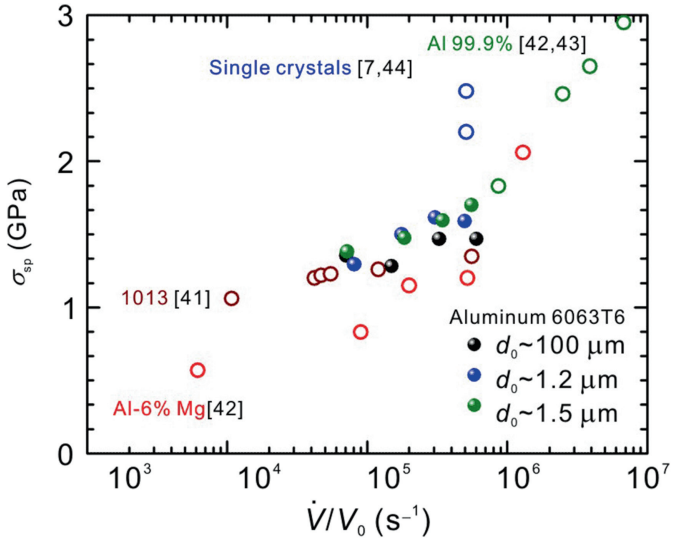

Fig. 9. Results of the measurements of spall strength of aluminum and aluminum alloys, carried out in this work and in Refs. [7,41–44], depending on the strain rate in the incident rarefaction wave.

Fig. 8 shows that after 2 passes, an increase of the Hugoniot elastic limit of the alloy AA6063T6 from 240 MPa to 400 MPa is observed. Further increase of the number of ECAP passes leads to its growth up to 520 MPa (i.e. more than twice). At the static deformation of this alloy, the authors of Ref. [38] noted an increase of the yield strength of the alloy 6063T6 by ~50% after 8 passes, associating this effect with the increased ductility of aluminum after a large number of ECAP passes. Dynamic strength of the alloy 6063T6 increases independently on the initial structure with increasing the strain rate. The decrease of the grain size after the procedure of severe plastic deformation in about 100 times led to an increase of spall strength of the alloy by about 15%. Thus, as expected, the number of ECAP passes did not affect it, since the average grain size with increasing number of ECAP passes has not changed, as its defect structure.

5.1.2. Aluminum alloy 1421

As another representative material with hcc structure, the aluminum alloy 1421 with a composition (in weight %) as Mg – 5, Li–2, Zr – 0.12, Sc – 0.2, and Al the rest, was tested. The nanostructured state in this alloy was also obtained by the method of ECAP (12 passes at 643 K). Before pressing, the alloy has been annealed at a temperature of 773 K for 30 min with the following quenching in water. After annealing with the following quenching, the alloy 1421 represents the supersaturated magnesium lithium solid solution with highly dispersed round particles in δ' phase (Al_3Li), as well as Al_3Zr and Al_3Sc with dimensions of 30–50 nm, distributed uniformly over the volume of the material. The grain size is ~7 μm. At the grain boundaries, there are also S phase particles (Al_2LiMg) with a size of 200–500 nm in small quantities. Equal channel angular pressing of the quenched alloy results in the grain refinement up to ~1.1 ± 0.4 μm. The grain acquires an equiaxial shape with high-angle disorientations. The dislocation density in them is about the same as that before ECAP processing. The particle sizes of the S and δ' phases are, respectively, 110–410 nm and 20–40 nm. The volume fraction of the particles of the S phase increases, and the particles are located primarily at the grain boundaries.

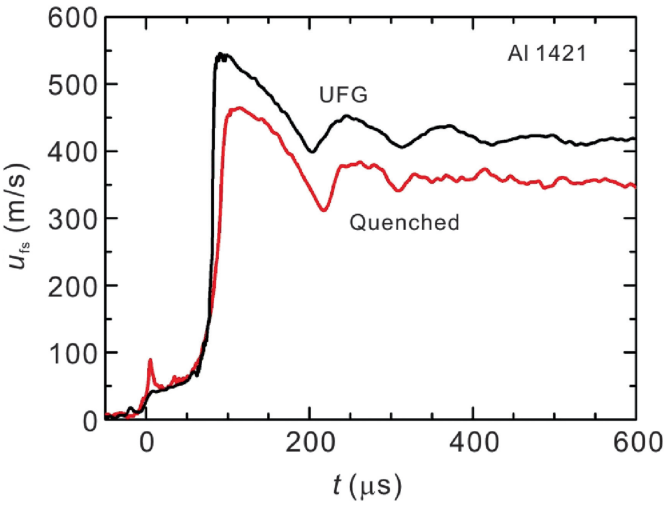

Fig. 10. Profiles of the free surface velocity of aluminum alloy 1421 samples in the quenched and deformed states by the method of ECAP. Loading of samples with a thickness of 2.7 mm was carried out by an impact of aluminum plate with a thickness of 0.4 mm at the velocity of 630 ± 30 m/s.

Fig. 10 presents the results of shock wave measurements for samples of this material. A sevenfold decrease in the grain size led to a ten percent increase of the quasi-static yield strength of the alloy and its small decreasing under the conditions of shock-wave loading. The wave profile for the quenched material demonstrates "yield drop" at the front of the elastic precursor, which is usually associated with intense multiplication of "the carriers of plastic deformation" – the dislocations at the initial stage of deformation. The grain refinement led to the disappearance of yield drop and a significant reduction of the rise time of the plastic shock wave indicating the reducing time of the stress relaxation. However, as can be seen from Fig. 10, the value of Δu_{fs} proportional to the spall strength of the material for the samples in different structural state is almost the same, i.e. the critical fracture stresses in this case do not depend on the structural state of the material.

5.2. Method of dynamic channel angular pressing

5.2.1. Aluminum alloys A7, A7075, A3003, A5083

In recent years, a new method of severe plastic deformation–Dynamic Channel Angular Pressing (DCAP) [45] has developed fast. By this method, the UFG materials (titanium, copper, brass, aluminum and its alloys) with improved mechanical properties [46–49] were obtained. Table 1 shows its characteristics in comparison with the classical method of ECAP. In this work, the results of the investigation of deformation behavior under shock compression of industrial as-received coarse-grained and ultrafine-grained aluminum alloys A7, A7075, A3003 and A5083 subjected to dynamic channel angular pressing are presented. The chemical composition, processing conditions by severe plastic deformation, the final average grain size and microhardness are presented in Table 2. By the analysis of the experimental free surface velocity profiles of the samples, their Hugoniot elastic limit σ_{HEL}, yield stress Y and the spall strength σ_{sp} at the strain rate (1.2–3) × 10^5 s^{-1} were obtained.

The study of the mechanical behavior of aluminum alloys, manufactured by DCAP, under dynamic compression in split Hopkinson-Kolsky pressure bar has identified a number of specific features, namely their enhanced dissipative ability and maintaining of high strength properties in the range of the strain rates (4–6) × 10^3 s^{-1} [50]. The mechanical

Table 1
The comparison of technical characteristics between classical ECAP and DCAP methods.

Characteristics	ECAP	DCAP
Strain rate	10^{-2} s^{-1}	10^4–10^5 s^{-1}
Deformation mode	Simple shear (tangential stresses)	Pressure pulse (normal stresses) + simple shear (tangential stresses)
Number of cycles required for UFG structure formation (with the average size of structural components of less than 500 nm)	6–8	1–2 (fraction of high-angle boundaries is more than 50%)
Material macroflow	Laminar	Laminar + turbulent
Density of lattice dislocations	10^{10}–10^{13} m^{-2}	10^{14}–10^{15} m^{-2}
Slip systems (planes)	Octahedral	Octahedral + nonoctahedral

Table 2
Characteristics of inner structure and parameters DCAP treatment of aluminum alloys tested.

Material tested	Commercial grade aluminum A7		Aluminum alloy A7075		Aluminum alloy A3003		Aluminum alloy A5083	
	As-received state	Ultra-fine grained	As-received state	Ultra-fine grained	As-received state	Ultra-fine grained	As-received state	Ultra-fine grained
Chemical composition (w%)	99.7Al-up 0.16 Fe-up 0.15 Si		Al-7.0Zn-2.3Mg-0.8Cu-0.5Si-0.5Fe-0.25Cr		Al–1.5Mn-0.1 Zn-0.05Cu-0.6 Si-0.7Fe		Al-4.4Mg-0.6Mn-0.11Si-0.23Fe-0.03Cr-0.02Cu- 0.06Ti	
DCAP treatment		V = ~200 m/s N = 4		V = ~150 m/s N = 1		V = ~200 m/s N = 1		V = ~300 m/s N = 1
Grain size	~180 μm	~700 nm	>2 μm	~200 nm	>2 μm	~500 nm	>2 μm	~240 nm
Microhardness (HB)	15	34–38	68	106	45	57–63	75	85

characteristics of these alloys under static loads with the decrease of grain size up to the submicron level in the aluminum increase by approximately 2.5 times.

The comparison of wave profiles for the CG and UFG samples of the same composition, processed under the same loading conditions, shows that for all alloys the transformation of the material into the UFG state is accompanied by an increase of Hugoniot elastic limit. The comparison of the amplitude and shape of the elastic precursor shows that the Hugoniot elastic limit σ_{HEL} proportional to the compressive stress behind the front of elastic precursor in the UFG alloys is always higher than the corresponding σ_{HEL} in CG analogs (approximately 1.5 times).

The Hugoniot elastic limit and spall strength of the investigated aluminum alloys A7, A3003 and A7075 in the as-received and UFG states are presented in Fig. 11. The highest growth of HEL was observed in aluminum A7, and the lowest – in alloy A3003. Accordingly, the dynamic yield strength of materials changes similarly. For UFG aluminum A7 compared to the CG analog, its 1.7 times increase took place for UFG alloys and A3003, A7075 – in 1.1 and 1.5 times, respectively. The growth of the dynamic yield strength of aluminum alloys at UFG structure, formed by the dynamic channel pressing, shows that the strengthen effect of DCAP method remains at the strain rate of ~10^5 s^{-1} under shock-wave loading. The UFG alloy A7075 has the highest value Y, while the UFG aluminum A7 – the lowest. Full accordance of the characteristics to each other is observed only in the alloy A7075 (in 1.5 times), but in alloy A3003, this deviation does not exceed 30%. Thus, all of the UFG aluminum alloys obtained by DCAP, at the strain rate of (1.2–3) × 10^5 s^{-1} show the increase of the elastic–plastic transition characteristics compared to the coarse-grain alloys. This distinguishes their behavior from UFG materials obtained by quasi-static techniques of SPD. For example, as seen from Fig. 10, the Hugoniot elastic limit of UFG aluminum alloy 1421, produced by ECAP is even lower in comparison with the quenched alloy. The similar result – a slight decrease of the dynamic yield stress is observed for tantalum UFG after multilateral forging [51] and titanium UFG obtained by ECAP [52], compared to the CG samples. The possible reason for such behavior of UFG aluminum alloys is their specific nonequilibrium structural state formed in the process of dynamic pressing as a result of the intensification of the fragmentation processes and dynamic recrystallization, as described above in detail.

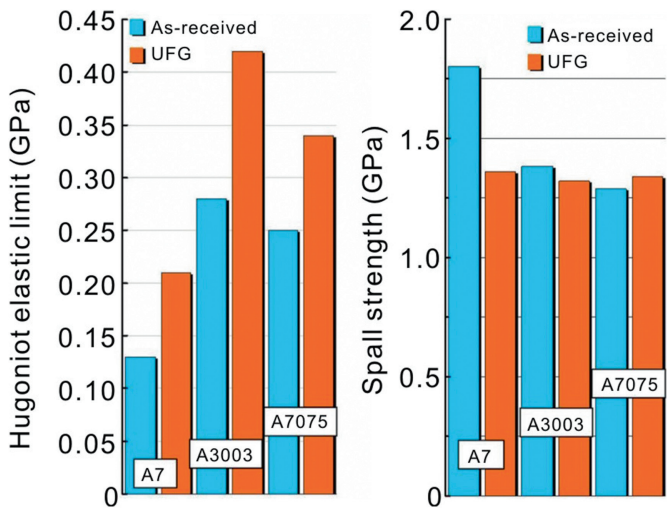

Fig. 11. Hugoniot elastic limit and spall strength of the investigated aluminum alloys A7, A3003 and A7075 in the as-received and UFG structural states.

The available literature data on the effect of the structure scale and degree of defectiveness on the resistance to spall fracture are ambiguous, and their correct comparison is possible only for the same strain rates. Thus, the reduction of grain size in tantalum to the UFG structure led to a 5% increase of spall strength [13], but in alloy 2024 [22] and copper [53], the authors found no difference in the process of dynamic fracture. The comparison of the results on the effect of grain size and defects structure in aluminum and its alloys on the spall strength obtained in this work is also not so unambiguous (Fig. 11). According to the conducted measurements, the absolute values of σ_{sp} of UFG materials are almost the same for all aluminum compositions and vary from 1.32 GPa to 1.36 GPa. The comparison of the critical fracture stresses at the spall of UFG and CG samples have shown that the transformation in the UFG state of A3003 alloy and aluminum A7 is accompanied by their decrease. In the doped alloy, the difference is only 7%, but in aluminum A7, the difference is substantially higher, 25%. If assuming that high-rate fracture at spall is a kinetic process of nucleation and growth of

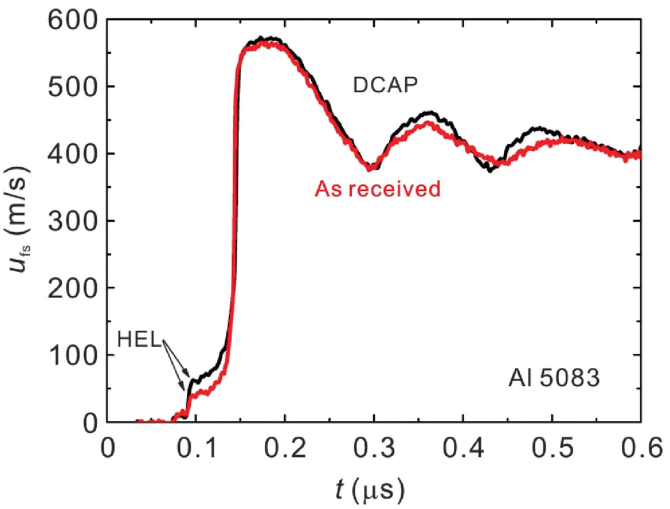

Fig. 12. Free surface velocity profiles for aluminum alloy A5083 in the as-received state and after severe plastic deformation by DCAP method. Sample thickness is ~2 mm, aluminum impactor is 0.4 mm in thickness at ~650 m/s.

defects concentrated in the grain boundaries and on the surface of the brittle intermetallic phases, the decrease of σ_{sp} of UFG materials is quite natural. In contrast to these two alloys, UFG alloy A7075 on the contrary shows a slight increase of spall strength. If comparing the values of spall strength of CG aluminum alloys and CG aluminum A7, higher values are found for the latter alloy (1.8 GPa vs. 1.34–1.38 GPa), as also noted in Ref. [42]. There it was approved that the difference in spall strength of polycrystalline aluminum of different purity and its alloys (for example, AMg6M) can be substantial and disappears only with the excess of the strain rate above 10^6 s^{-1}. It is necessary to add that the calculated wave profile thickness of the spall plate in all UFG alloys varies in the range of 0.3–0.4 mm, which is ~10% less than in analogous coarse-grain alloys.

In Fig. 12 the wave profiles obtained in the shock-wave experiments with samples of aluminum alloy A5083 in the as-received state and after severe plastic deformation by DCAP method are presented. As in the case of other alloys, the reduction of grain sizes in alloy A5083 after DCAP treatment leads to the growth of its Hugoniot elastic limit in about 1.5 times in comparison with the alloy in the as-received state, for which this value is 0.31 GPa. The critical fracture stresses at spall are almost the same for both aluminum structure states and are ~1.39 GPa. The strain rate before the fracture in these experiments do not exceed ~2 × 10^5 s^{-1}. Thus, it is possible to note that this alloy shows the largest increase of Hugoniot elastic limit and the lowest sensitivity of spall strength at the radical reduction of the average grain size after severe plastic deformation among the studied aluminum alloys.

5.3. Method of High-Pressure Torsion

5.3.1. Aluminum alloy 5053

Apparently, one of the first methods of severe plastic deformation suggested by P. W. Bridgman in the late forties of the last century was the so-called method of High-Pressure Torsion (HPT) [54–56]. Here are the results of researches of behavior of the same industrial alloy A5083, the samples of which were investigated after DCAP treatment (see subsec. 5.2), under dynamic loading after severe plastic deformation by HPT method. In the coarse-crystal state, the alloy was an industrial hot-pressed rod in the annealed state with the hardness $HB = 75$. To obtain samples with the ultrafine-grained structure in this case, the method of torsion under pressure (HTP), a flat disc with a diameter of 20 mm and a thickness of 1 mm at the strain rate of ~10^{-2} s^{-1} was used. Several kinds of samples with the number of turnarounds of the anvil $n = 1$, 5 and 10 were prepared, corresponded to the accumulated strain of $\varepsilon = 7.0$, 8.6 and 9.3, respectively. Electron microscopic study of the sample structure has shown that a strong refinement of the structure has already been observed at the initial deformation $\varepsilon = 7.0$. The fragmented structure was formed, the major part of which was deformed grains with internal nonuniform contrast and blurred high-angled boundaries, and with the high level internal stresses. With the increase of the degree of accumulated deformation, the morphological peculiarities of structure formation were saved, and the process of fragmentation was further developed. Mostly high-angle boundaries were formed in the structure. According to the results of X-ray diffraction analysis, with increasing the accumulated deformation in the material, the density of lattice dislocations increased from 7.8 × 10^{13} to 2.6 × 10^{14} m^{-2}. The accumulation of defects changed the dislocation ensemble as a whole: the interaction of dislocations with low-angle boundaries activates, the disorientation of deformation boundaries increased, mesodefects but disclinations appeared in the triple junctions of grain boundaries, and rotational modes of plasticity development.

With the growth of the accumulated deformation, the range of grain size was narrowing down; the part of large crystallites larger than 450 nm was decreasing, i.e. the structure became more uniform. The average size of the grains-subgrains with 170–180 nm for $\varepsilon \leq 8.6$ was reduced to the nano-level of ~100 nm at $\varepsilon = 9.3$. The observed evolution of the structure with increasing deformation agreed with the data on hardness. In comparison with the initial state, the hardness increased in 2.5 times, reaching the value of 2500 MPa at $n = 10$. Assuming that various mechanisms of hardening make their contributions additively, the increase in hardness of the deformed UFG alloy was due to the grain boundary and dislocation components of hardening, as at the HPT treatment, in which the processes of deformation and dissolution of intermetallics or dynamic aging of the matrix were not recorded.

The shock wave experiments with samples of 1 mm thick in initial, ultrafine-grained and nanocrystalline states at the impact with aluminum foil of thickness of 0.21 mm were conducted, using the experimental setups shown in Fig. 1. The strain rate of aluminum alloy before the spall in these experiments was ~4.0 × 10^5 s^{-1}. Table 3 presents the results of the measurements of dynamic strength characteristics of aluminum alloy A5083 in the initial state and after deformation by HPT method.

Table 3
Dynamic strength properties of the alloy A5083 after HPT processing.

Structure	n	ε	σ_{HEL} (GPa)	Y (GPa)	σ_{sp} (GPa)
CG		−	0.37	0.19	1.52
UFG	1	7.0	0.77	0.42	1.13
UFG	5	8.6	0.78	0.43	1.18
NC	10	9.3	0.85	0.47	1.44

As from Table 3, it can be seen that the values of the Hugoniot elastic limit and the dynamic yield stress of UFG samples obtained by HPT method ($\varepsilon = 7.0$ and 8.6, respectively) compared to the coarse-grained analog, are two times higher than these characteristics of the initial samples. The structure refinement up to the nanoscale ($n = 10$, $\varepsilon = 9.3$) leads to a further rise of σ_{HEL} and Y approximately by 10%. Thus, the obtained values of the characteristics are correlated with the changes in grain sizes. In contrast, the value of the critical fracture stresses σ_{sp} is unambiguously not connected to the scale of the structures obtained by HPT method. Severe plastic deformation significantly reduces its value, and only in nanostructured samples the spall strength increases again up to close to the initial values.

To understand and explain these results, it is necessary to analyze the differences in the structure of alloys, deformed by different methods. If not taking into account the small difference in the average size of the structural components, namely, 240 nm for UFG alloy obtained by DCAP method, and 150−200 nm for UFG alloy after HPT ($n = 1, 5$), the main factors of the difference are the ratio of low-angle and high-angle boundaries and the density of defects. Both of these factors contribute to the total strengthening of the alloy, and regulate the value of the dynamic yield stress. On the basis of the obtained values of Y, it follows that, despite the lower dislocation density in the UFG structure after HPT, the higher values of yield stress (80 MPa) are achieved due to the grain-boundary hardening caused by the formation of a bigger part of grains with high-angle disorientation. The transformation to a nanostructure, when $n = 10$, $\varepsilon = 9.3$, and the increase in the length of non-equilibrium boundaries aggravate this difference up to 140 MPa. It is also a proof of correctness of the discovered regularities. Therefore, compared to the samples deformed by HPT, the samples after DCAP demonstrate lower dynamic characteristics. The spall strength of the alloy after DCAP coincides with the spall strength of the CG alloy and is 1.5 GPa. According to the amplitude and the shape of the spall pulse, the fracture rates of these materials are also close to each other.

5.4. Method of Accumulative Roll-Bonding

5.4.1. Aluminum alloy AA1070

At the very end of the last century, the method of production of ultrafine-grained materials by multiple rolling of specially prepared sheets of metals with their subsequent bonding was proposed [57,58]. As a result of this technology, the "sandwich" of several metal layers with fined grain structure repeatedly rolled was produced. This method, called Accumulative Roll-Bonding (ARB), allows obtaining ultrafine-grained sheet of the workpiece, which is large enough, already suitable for the manufacture of various parts and components of machinery requiring high tensile strength. In this paper, the results of the investigation of strength characteristics of aluminum alloy AA1070 in the initial CG state and after severe plastic deformation by the ARB method [58] are presented. The chemical composition of the alloy AA1070 measured by X-ray microanalysis with the use of wave spectrometer was 0.25% Si, 0.02% Fe, 0.01% Cu, 0.01% Mn, 0.01% Ti and the rest, aluminum. Before rolling, the sheet workpiece was subjected to recrystallized annealing at the temperature of 773 K for 1 h. Then the material in the form of two bands with the thickness of 1 mm, the width of 30 mm and the length of 300 mm was washed in acetone, subjected to a surface treatment with a wire brush, collected into a "package" and rolled at room temperature to 50% at a speed of 0.1 m/s. The obtained band was cut in half along the length. This sequence was considered as 1 cycle of rolling with banding of layers. In the whole, there were 4 workpieces of material subjected to 4, 7, 10 and 14 cycles of rolling. The degree of the accumulated true strain was 3.2, and 5.6 and 8.0, and 11.2, respectively.

Fig. 13 presents the results of structural studies of AA1070 alloy in the recrystallized (initial) state and after ARB processing after 4, 7 and 10 cycles. It is seen that after 4 cycles, the average grain size decreases drastically − from ~98 μm to ~6 μm. After 10 cycles of rolling, it decreases slightly on average up to ~2 μm. The microhardness of the alloy also changes sharply from ~350 MPa for the initial state up to 550−600 MPa for the other samples after rolling. The part of high-angled boundaries varies depending on the number of the rolling cycles not so radically and, as it can be seen from the figure, initially it decreases by about 20%, and after 10 cycles, its value is almost back to initial. Fig. 14 shows the results of the measurements of mechanical characteristics of aluminum AA1070 − tensile strength σ_{max}, yield stress Y and deformation before fracture δ. Flow stress in the region of the elastic−plastic transition Y and the strength in the loss of stability of the sample σ_{max} quite smoothly increases with the number of cycles of rolling, and only after 14 cycles their values decrease a little. The deformation ability of the alloy is greatly reduced to almost zero immediately after four times rolling, staying at the level of a few percent when increasing their number up to 10, and only after 14 cycles of rolling the deformation ability of the material increases again to about 15%.

The dependencies of the strength characteristics of aluminum AA1070 on the number of cycles ARB processing are shown in Fig. 15. It is seen that the value of the Hugoniot elastic limit increases in about 4 times (from 78 MPa in the recrystallized material up to 300 MPa) as a result of 4 cycles of rolling. After increasing the number of cycles up to 7, the value of HEL remains practically unchanged. After 10 cycles of rolling, it increases by 15%−350 MPa and then begins to decline slightly. It should be noted that, as with other metals

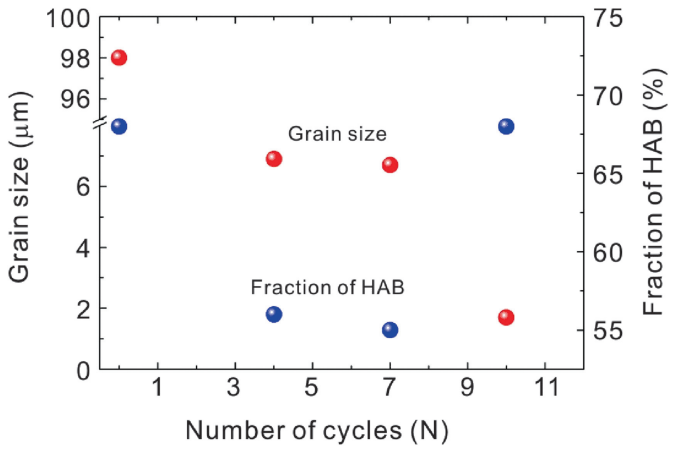

Fig. 13. Dependence of the average grain size and parts of high-angled grain boundaries on the number of cycles of accumulative rolling.

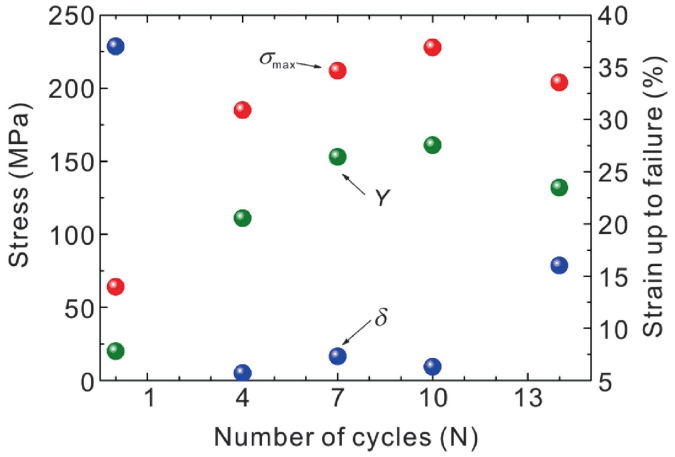

Fig. 14. Dependences of strength (σ_{max}), yield strength (Y) and also strain up to fracture (δ) on the number of cycles of accumulative rolling.

and methods of manufacturing of UFG materials, the increase of yield strength under static and quasi-static testing is much higher (up to 5.5 times). These results agree with the results of the investigations for aluminum alloys A7, A7075 and A3003 in ultrafine-grained state after DCAP presented above. Thus, one can conclude that under the conditions of dynamic loadings, the presence of a large number of internal interfaces generated by the bonding of the material by ARB method has no negative effect on the strength properties of the material.

Unlike the Hugoniot elastic limit of the aluminum, after 4 cycles of rolling, the value of the spall strength decreases significantly, remaining approximately constant with the increasing of the number of cycles up to 7, and then reaches a minimum value at the number of cycles of rolling 10. At the further increase of the number of the rolling cycles, the value of the spall strength slightly increases. The variations of the spall strength of these aluminum specimens subjected to ARB are small compared with its sharp decreasing in relation to the strength of the non-rolled samples, if taking into account the scatter of data for samples of the same type. One can assume

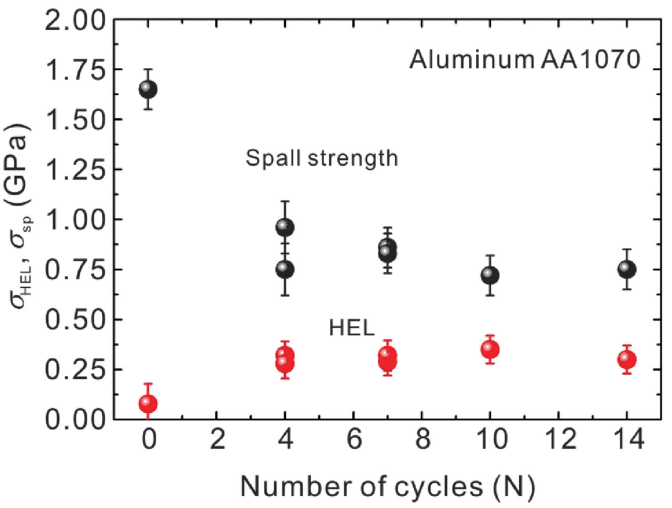

Fig. 15. Spall strength and Hugoniot elastic limit of aluminum alloy AA1070 in different structural states after ARB processing.

that such a strong decrease in strength of the samples after SPD is connected with the presence in the structure of deformed samples of a large number of induced defects by the rolling process, which were the initiators of the formation of spall crack, i.e. fracture of the sample. A weak dependence of fracture stresses on the number of rollings suggests that from the point of view of a spall fracture, which occurs in the material volume, the structures of the samples be similar.

In these experiments, the variations of the thickness of the spall plate from sample to sample are observed, despite almost identical ratio of the impactor thickness to the thickness of the sample (0.21 mm/~1 mm in all experiments). In this case, the thickness of the spall plate according to the wave interactions inside the sample should be close to the impactor thickness as a result of practically identical compressibility of the material of the impactor and the sample. However, its calculations from the wave profiles show that this condition is fulfilled only for the initial undeformed samples with a minimum number of defects. In all other cases, sample thickness is smaller and it varies from sample to sample, which is, obviously, associated with the presence of induced defects distributed non-uniformly across the volume in the structure of deformed samples. The nucleation of spall crack occurs in the most defective section at achieving significantly lower values of tensile stresses, as is seen from Fig. 15.

6. Conclusion

The recent studies confirm the informativeness and usefulness of shock wave testing of materials and, in some cases, demonstrate the non-trivial nature of their high-rate fracture. The experiments with shock waves allow obtaining information about the most fundamental strength properties of materials in conditions excluding the influence of the surface on the processes of deformation and fracture. Due to this, in solids it is possible to realize the conditions close to the maximum possible strength, and thus to evaluate experimentally their strength resource. The

results of the investigations presented here clearly demonstrate the influence of structural factors on resistance to high-rate deformation and fracture, but it is much less than under the static and quasi-static loading. It seems to be useful in the future to formalize the results of the spall strength measurements by introducing ideas about the spectrum of potential sources of fracture in the material characterized by different stress levels necessary for activation. It is hoped that this approach will provide a more detailed description of the strength properties of materials and increase the informativity of studies at high strain rates.

Conflict of interest

No conflict of interest.

Acknowledgments

This work was carried out within the state tasks No. 0089-2014-0016 and it was also supported by the Program No. 11P of basic researches of Presidium of Russian Academy of Sciences “Condensed matter and plasma at high energy densities. Physics and mechanics of deformation and fracture with extremely high rates”.

References

[1] T. Antoun, L. Seaman, D.R. Curran, G.I. Kanel, S.V. Razorenov, et al., Spall Fracture, Springer, New York, 2003, 404 pp.
[2] G.I. Kanel, S.V. Razorenov, A.V. Utkin, V.E. Fortov, Shock-wave Phenomena in Condensed Matter, Yanus-K, Moscow, 1996, 407 pp. (In Russian).
[3] Ya.B. Zel'dovich, Yu.P. Raizer, Physics of Shock Waves and High-temperature Hydrodynamic Phenomena, vol. I, Academic Press, New York, 1966.
[4] G.I. Kanel, S.V. Razorenov, V.E. Fortov, Shock-wave Phenomena and the Properties of Condensed Matter, Springer, New York, 2004, 321 pp.
[5] L.M. Barker, R.E. Hollenbach, Laser interferometry for measuring high velocities of any reflecting surface, J. Appl. Phys. 43 (1972) 4669−4675.
[6] G.V. Garkushin, G.I. Kanel, S.V. Razorenov, Deformation and breaking strength of aluminum AD1 for a shock wave stress at temperatures of 20 and 600°C, Phys. Solid State 52 (11) (2010) 2369−2375.
[7] G.I. Kanel, S.V. Razorenov, K. Baumung, J. Singer, Dynamic yield and tensile strength of aluminum single crystals at temperatures up to the melting point, J. Appl. Phys. 90 (1) (2001) 136−143, https://doi.org/10.1063/1.1374478.
[8] S.P. Marsh, LASL Shock Hugoniot Data, Berkeley, University of California Press, 1980, 658 pp.
[9] G.I. Kanel, Spall fracture: methodological aspects, mechanisms and governing factors, Int. J. Fract. 163 (1−2) (2010) 173−191.
[10] S.V. Razorenov, G.I. Kanel, The strength of copper single crystals and the factors governing metal fracture in uniaxial dynamic stretching, Phys. Met. Metallogr. 74 (5) (1992) 526−530.
[11] G.I. Kanel, S.V. Razorenov, A.V. Utkin, V.E. Fortov, K. Baumung, et al., Spall strength of molybdenum single crystals, J. Appl. Phys. 74 (12) (1993) 7162−7165.
[12] A.A. Bogach, G.I. Kanel, S.V. Razorenov, A.V. Utkin, S.G. Protasova, V.G. Sursaeva, Resistance of zinc crystals to shock deformation and fracture at elevated temperatures, Phys. Solid State 40 (10) (1998) 1676−1680.
[13] S.V. Razorenov, G.I. Kanel, G.V. Garkushin, O.N. Ignatova, Resistance to dynamic deformation and fracture of tantalum with different grain and defect structures, Phys. Solid State 54 (4) (2012) 790−797, https://doi.org/10.1134/S1063783412040233.
[14] S.V. Razorenov, A.S. Savinykh, E.B. Zaretsky, Elastic-plastic deformation and fracture of shock-compressed single-crystal and polycrystalline copper near melting, Tech. Phys. 58 (10) (2013) 1437−1442, https://doi.org/10.1134/S1063784213100216.
[15] G.I. Kanel, G.V. Garkushin, A.S. Savinykh, S.V. Razorenov, T. de Resseguier, et al., Shock response of magnesium single crystals at normal and elevated temperatures, J. Appl. Phys. 116 (2014), 143504, https://doi.org/10.1063/1.4897555.
[16] G.I. Kanel, E.B. Zaretsky, S.V. Razorenov, S.I. Ashitkov, V.E. Fortov, Unusual plasticity and strength of metals at ultra-short load durations, Phys. Usp. 60 (5) (2017) 490−508, https://doi.org/10.3367/UFNe.2016.12.038004.
[17] S.I. Ashitkov, P.S. Komarov, A.V. Ovchinnikov, E.V. Struleva, M.B. Agranat, Deformation dynamics and spallation strength of aluminium under a single-pulse action of a femtosecond laser, Quant. Electron. 43 (3) (2013) 242−249, https://doi.org/10.1070/QE2013v043n03ABEH015104.
[18] S.I. Ashitkov, M.B. Agranat, G.I. Kanel, P.S. Komarov, V.E. Fortov, Behavior of aluminum near an ultimate theoretical strength in experiments with femtosecond laser pulses, J. Exp. Theor. Phys. Lett. 92 (2010) 516−520, https://doi.org/10.1134/S0021364010200051.
[19] G.V. Sin'ko, N.A. Smirnov, Ab initio calculations of the equation of state and elastic constants of aluminum in the region of negative pressures, J. Exp. Theor. Phys. Lett. 75 (3) (2002) 184−186, https://doi.org/10.1134/1.1475719.
[20] V.D. Glusman, G.I. Kanel, V.F. Loskutov, V.E. Fortov, I.E. Khorev, Resistance to deformation and fracture of 35Kh3NM steel under conditions of shock loading, Strength Mater. 17 (8) (1985) 1093−1099.
[21] S.V. Razorenov, A.A. Bogach, G.I. Kanel, The effect of heat treatment and polymorphic transformations on the dynamic strength of steel 40 Kh, Phys. Met. Metallogr. 83 (1) (1997) 100−103.
[22] G.V. Garkushin, S.V. Razorenov, G.I. Kanel, Effect of structural factors on submicrosecond strength of D16T aluminum alloy, Tech. Phys. 53 (11) (2008) 1441−1446, https://doi.org/10.1134/S1063784208110078.
[23] V.A. Ogorodnikov, E.Yu. Borovkova, S.V. Erunov, Strength of some grades of steel and Armco iron under shock compression and rarefaction at pressures of 2−200 GP, Combust. Explos. Shock Waves 40 (5) (2004) 597−604.
[24] G.T. Gray III, N.K. Bourne, A.M. Zocher, P.J. Maudlin, J.C.F. Millett, Influence of crystallographic anisotropy on the Hopkinson fracture “spallation” of zirconium, in: M.D. Furnish, L.C. Chhabildas, R.S. Hixson (Eds.), Shock Compression of Condensed Matter-1999, AIP Press, Woodbury, NY, 2000, pp. 509−512.
[25] G.T. Gray III, M.F. Lopez, N.K. Bourne, J.C.F. Millett, K.S. Vecchio, Influence of microstructural anisotropy on the spallation of 1080 eutectoid steel, in: M.D. Furnish, N.N. Thadhani, Y. Horie (Eds.), Shock Compression of Condensed Matter-2001, AIP Press, Melville, NY, 2002, pp. 479−482.
[26] K. Baumung, G.I. Kanel, S.V. Razorenov, D. Rusch, J. Singer, et al., Investigations of the dynamic strength variations in metals, J. Phys. 7 (1997) C3−C927. IV France.
[27] M.D. Furnish, W.D. Reinhart, W.M. Trott, L.C. Chhabildas, T.J. Vogler, Variability in dynamic properties of tantalum: spall, Hugoniot elastic limit and attenuation, in: M.D. Furnish, et al. (Eds.), Shock Compression of Condensed Matter − 2005, AIP Conference Proceedings, vol. 845, 2006, pp. 615−618. New York.
[28] M.A. Meyers, D.J. Benson, O. Vohringer, B.K. Kad, Q. Xue, et al., Constitutive description of dynamic deformation: physically-based mechanisms, Mater. Sci. Eng. A322 (2002) 194−216.
[29] E.O. Hall, The deformation and ageing of mild steel: III discussion of results, Proc. Phys. Soc. B 64 (1951) 747−753.
[30] N.J. Petch, The cleavage strength of polycrystals, J. Iron Steel 174 (1953) 25−28.
[31] R.Z. Valiev, N.A. Enikeev, M. Yu. Murashkin, S.E. Aleksandrov, R.V. Goldshtein, Superstrength of ultrafine grained aluminum alloys produced by severe plastic deformation, Dokl. Phys. 55 (6) (2010) 267−270, https://doi.org/10.1134/S1028335810060054.
[32] T.G. Langdon, Ultrafine-grained materials: a personal perspective, Int. J. Mater. Res. 98 (4) (2007) 251−254.

[33] Y. Estrin, A. Vinogradov, Extreme grain refinement by severe plastic deformation: a wealth of challenging science, Acta Mater. 61 (2013) 782−817.
[34] R.Z. Valiev, R.K. Islamgaliev, I.V. Alexandrov, Bulk nanostructured materials from severe plastic deformation, Prog. Mater. Sci. 45 (2000) 103−189.
[35] G.A. Malygin, Strength and plasticity of nanocrystalline materials and nanosized crystals, Physics Usp 54 (2011) 1091−1116, https://doi.org/10.3367/UFNe.0181.201111a.1129.
[36] M.A. Meyers, A. Mishra, D.J. Benson, Mechanical properties of nanocrystalline materials, Prog. Mater. Sci. 51 (2006) 427−556.
[37] M. Hockauf, L.W. Meyer, T. Hprin, M. Hietschold, S. Schultze, et al., Mechanical properties and microstructural changes of ultrafine-grained AA6063T6 during high-cycle fatigue, Int. J. Mater. Res. 97 (10) (2006) 1392−1400.
[38] L.W. Meyer, M. Hockauf, L. Krüger, I. Schneider, Compressive behavior of ultrafine-grained AA6063T6 over a wide range of strains and strain rates, Int. J. Mater. Res. 98 (3) (2007) 1−9.
[39] J.M. Winey, B.M. LaLone, P.B. Trivedi, Y.M. Gupta, Elastic wave amplitudes in shock-compressed thin polycrystalline aluminum samples, J. Appl. Phys. 106 (2009), 073508.
[40] T.E. Arvidsson, Y.M. Gupta, G.E. Duvall, Precursor decay in 1060 aluminum, J. Appl. Phys. 46 (1975) 4474−4481.
[41] G.I. Kanel, S.V. Razorenov, A.A. Bogatch, A.V. Utkin, V.E. Fortov, et al., Spall fracture properties of aluminum and magnesium at high temperatures, J. Appl. Phys. 79 (11) (1996) 8310−8317.
[42] S.V. Razorenov, G.I. Kanel, V.E. Fortov, Submicrosecond strength of aluminum and an aluminum-magnesium alloy AMg6M at normal and enhanced temperatures, Phys. Met. Metallogr. 95 (1) (2003) 86−91.
[43] K. Baumung, H. Bluhm, G.I. Kanel, G. Müller, S.V. Razorenov, et al., Tensile strength of five metals and alloys in the nanosecond load duration range at normal and elevated temperatures, Int. J. Imp. Eng. 25 (7) (2001) 631−639.
[44] G.I. Kanel, S.V. Razorenov, Anomalies in the temperature dependences of the bulk and shear strength of aluminum single crystals in the submicrosecond range, Phys. Solid State 43 (5) (2001) 871−877.
[45] E.V. Shorokhov, I. N. Zhgilev, R.Z. Valiev, Method of dynamic treatment of materials. RF Patent 2283717. Byull. Izobret., 26 (2006).
[46] I.V. Khomshaya, E.V. Shorokhov, V.I. Zel'dovich, A.E. Kheifets, N.Yu. Frolova, et al., Study of the structure and mechanical properties of submicrocrystalline and nanocrystalline copper produced by high-rate pressing, Phys. Met. Metallogr. 111 (6) (2011) 612−622.
[47] V.I. Zel'dovich, E.V. Shorokhov, N.Yu. Frolova, et al., High-rate deformation of titanium subjected to dynamic channel-angular pressing, Phys. Met. Metallogr. 105 (4) (2008) 402−408.
[48] V.I. Zel'dovich, I.V. Khomskaya, N.Yu Frolova, A.E. Kheifets, E.V. Shorokhov, et al., Structure of chromium-zirconium bronze subjected to dynamic channel-angular pressing and aging, Phys. Met. Metallogr. 114 (5) (2013) 411−418.
[49] I.G. Brodova, A.N. Petrova, I.G. Shirinkina, E.V. Shorokhov, I.V. Minaev, et al., Fragmentation of the structure in Al-based alloys upon high speed effect, Rev. Adv. Mater. Sci. 25 (2) (2010) 128−135.
[50] A.N. Petrova, I.G. Brodova, O.A. Plekhov, O.B. Naimark, E.V. Shorokhov, Mechanical properties and energy dissipation in ultrafine-grained AMts and V95 aluminum alloys during dynamic compression, Tech. Phys. 59 (7) (2014) 989−996, https://doi.org/10.1134/S1063784214070226.
[51] M.V. Aniskin, O.N. Ignatova, I.I. Kaganova, A.V. Kalmanov, E.V. Koshatova, et al., Mechanical properties of tantalum with different types of microstructure under high-rate deformation, Phys. Mesomech. 14 (1) (2011) 79−84, https://doi.org/10.1016/j.physme.2011.04.010.
[52] S.V. Razorenov, A.S. Savinykh, E.B. Zaretsky, G.I. Kanel, Yu.R. Kolobov, Effect of preliminary strain hardening on the flow stress of titanium and a titanium alloy during shock compression, Phys. Solid State 47 (4) (2005) 663−669.
[53] G.V. Garkushin, G.E. Ivanchikhina, S.V. Razorenov, O.N. Ignatova, A.N. Malyshev, et al., Mechanical properties of grade M1 copper before and after shock compression in a wide range of loading duration, Phys. Met. Metallogr. 111 (2) (2011) 197−206.
[54] P.W. Bridgman, On torsion combined with compression, J. Appl. Phys. 14 (1943) 273−283, https://doi.org/10.1063/1.1714987.
[55] P.W. Bridgman, The effect of hydrostatic pressure on plastic flow under shearing stress, J. Appl. Phys. 17 (1946) 692−697, https://doi.org/10.1063/1.1707772.
[56] P.W. Bridgman, Studies in Large Scale Plastic Flow and Fracture, McGraw-Hill, New York, NY, 324 pp.
[57] Y. Saito, N. Tsuji, H. Utsunomiya, T. Sakai, R.G. Hong, Ultra-fine grained bulk aluminum produced by accumulative roll-bonding (ARB) process, Scripta Mater. 39 (9) (1998) 1221−1227, https://doi.org/10.1016/S1359-6462(98)00302-9.
[58] Y. Saito, H. Utsunomiya, N. Tsuji, T. Sakai, Novel ultra-high straining process for bulk materials—development of the accumulative roll-bonding (ARB) process, Acta Mater. 47 (2) (1999) 579−583, https://doi.org/10.1016/S1359-6454(98)00365-6.